MacPherson Suspension System Modeling and Control with MDP

Enso Ikonen[1,*], Kaddour Najim and Alfonso García-Cerezo[2]

Abstract— **Simulation-based non-linear active suspension control design for MacPherson systems is considered. A non-linear dynamic model for the MacPherson suspension system is derived. The model nonlinearities and the dynamic behaviour of the system is illustrated by simulations. The design of controllers and state estimators using finite state Markov models is briefly outlined, and applied for nonlinear active suspension control system. The study illustrates the potential of the finite Markov chains approach in non-linear active suspension control, emphasizing the possibility to move computational load due to simulations to off-line design.**

I. Introduction

Active suspension control has been a topic of intensive academic research for several decades. The active (or semi-active) control systems have become an important tool for reaching better ride comfort and handling performance. With the increasing robustness and decreasing price of sensors, communication, and computing power in modern vehicles, more and more complex systems are being considered for practical implementations.

The main requirements of vehicle suspension systems [1] are related to ride comfort (vs. road roughness), vehicle handling (agility) and posture (when subject to breaking, turning, etc), and suspension stroke limits. These can be expressed in terms of sprung mass acceleration (ride comfort), tyre deflection (vehicle handling), and suspension deflection (rattle space). Most advanced control concepts are model-based, and consequently dynamic modelling of the system plays a key role. Active suspension system modelling then considers the dynamic components of the system consisting of springs, dampers and actuators in various configurations, leading to quantification of performance objectives. LQ optimal control is particularily popular and usually based on the linear quarter-car model. Cao et al [2] review intelligent active suspension control systems, which typically involve non-linear components.

The MacPherson suspension [3][4] is widely used in small and medium sized vehicles and poses a challenging problem due to its nonlinear asymmetric behaviour. The variable geometry provokes a nonlinear behaviour related to both kinematics and dynamics. While modelling the system as a three dimensional one is a complex problem and simulations are computationally expensive, a two-dimensional planar model can capture the nonlinear effects of the McPherson suspension. In this paper, a dynamic model for a MacPherson suspension system is developed by analysing the system kinematics and deriving the dynamics using the Euler-Lagrange approach. The text is inspired by the paper by Hurel and co-authors [4], but the resulting expressions are significantly simpler than in [4] or [3], making the model attractive for simulation-based nonlinear control design. The model is applied for the design of a finite state and action optimal controller using Markov chains modelling and value iteration for solving the optimal controller.

The reminder of the paper is structured as follows. The next Section derives the model equations by examination of system kinematics and dynamics via the Euler-Lagrange equations. The model nonlinearities are illustrated by plots in Section III, and dynamic behaviour of the system is simulated with kerbstrike and pothole road profiles. The second half of the paper describes the design of a finite state and action Markov chain based optimal controller (Sec IV) applied for active suspension control (Sec V). The performance of the active and passive systems is compared in simulations. A summary and discussion ends the paper.

II. Derivation of the model equations

The set-up and notation used in the modelling of the MacPherson suspension system are adopted from [4], and shown in Figs. 1-2. The sprung mass connection points are Q and M. Suspension key points in a plane are denoted by C (center of wheel assembly) and P (control arm). The origo of the y-z-coordinate system is in point Q_0, where subscript '0' denotes the initial equilibrium position. The points in the plane can be defined by Cartesian coordinates (Y_i, Z_i), $i = \{C, P, Q, M\}$. In addition, two angles ϕ (camber angle) and θ (control arm) are shown in the figure. The angle θ is positive anticlock-wise, while the camber angle ϕ is by convention positive clock-wise. The generalized coordinates are vertical displacements of the sprung mass Z_s and unsprung mass Z_u, Z_r is the vertical displacement of the road.

A. Kinematics

System kinematics are obtained with 'matrix displacement method' [3] [4]:

$$\begin{bmatrix} Y_N & Y_T & Y_P \\ Z_N & Z_T & Z_P \\ 1 & 1 & 1 \end{bmatrix} = \mathbf{A} \begin{bmatrix} Y_{N0} & Y_{T0} & Y_{P0} \\ Z_{N0} & Z_{T0} & Z_{P0} \\ 1 & 1 & 1 \end{bmatrix}$$

where

$$\mathbf{A} = \begin{bmatrix} \cos\phi & \sin\phi & Y_C - (Y_{C0}\cos\phi + Z_{C0}\sin\phi) \\ -\sin\phi & \cos\phi & Z_C - (Z_{C0}\cos\phi - Y_{C0}\sin\phi) \\ 0 & 0 & 1 \end{bmatrix}$$

[1]E. Ikonen and K. Najim are with the University of Oulu, Systems Engineering, POB 4300, FIN-90014 University of Oulu, Finland enso.ikonen@oulu.fi

[2]A. García-Cerezo is with the Departamento de Ingeniería de Sistemas y Automática, Universidad de Málaga, Spain

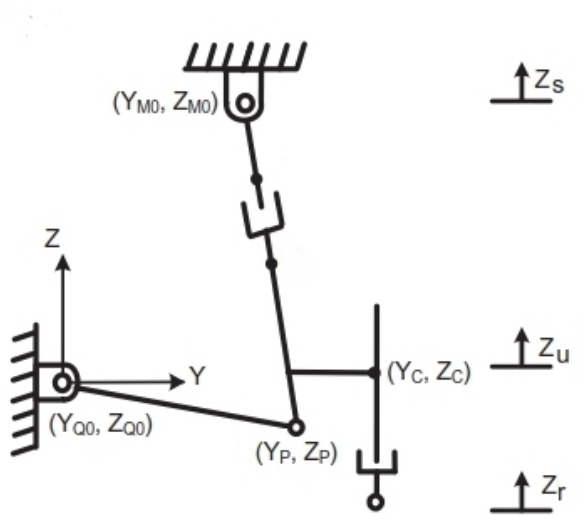

Fig. 1. Kinematic model.

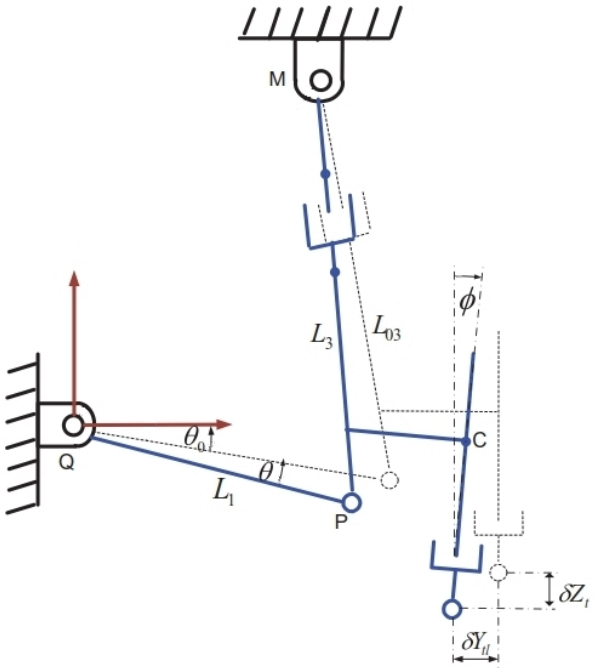

Fig. 2. Suspension motion.

from where the relation betwen points P and C can be written as

$$\begin{aligned} Y_P - Y_C &= (Y_{P0} - Y_{C0})\cos\phi + (Z_{P0} - Z_{C0})\sin\phi \\ Z_P - Z_C &= (Z_{P0} - Z_{C0})\cos\phi - (Y_{P0} - Y_{C0})\sin\phi \end{aligned}$$

Assuming small angles ($\cos\phi \simeq 1$ and $\sin\phi \simeq \phi$) leads to

$$Y_P - Y_C \simeq (Y_{P0} - Y_{C0}) + (Z_{P0} - Z_{C0})\,\phi \quad (1)$$
$$Z_P - Z_C \simeq (Z_{P0} - Z_{C0}) - (Y_{P0} - Y_{C0})\,\phi \quad (2)$$

Assume that the chassis moves only in the vertical dimension,

$$Z_Q = Z_{Q0} + Z_s, \quad (3)$$
$$Y_Q = Y_{Q0} \quad (4)$$
$$Z_M = Z_{M0} + Z_s \quad (5)$$
$$Y_M = Y_{M0} \quad (6)$$

and

$$Z_C = Z_{C0} + Z_u \quad (7)$$

For the point P, the system geometry gives

$$\begin{aligned} Y_P &= L_1\cos(\theta_0 + \theta) \\ Z_P &= L_1\sin(\theta_0 + \theta) + Z_s \end{aligned}$$

Using the angle summation rules for cosine and sine: $\cos(\theta_0 + \theta) = \cos\theta_0\cos\theta - \sin\theta_0\sin\theta$ and $\sin(\theta_0 + \theta) = \sin\theta_0\cos\theta + \cos\theta_0\sin\theta$ and assuming small angles, an approximation is obtained:

$$\begin{aligned} Y_P &\approx L_1\cos\theta_0 - (L_1\sin\theta_0)\,\theta \\ Z_P &\approx L_1\sin\theta_0 + (L_1\cos\theta_0)\,\theta + Z_s \end{aligned}$$

Since Q_0 is the origo, we have that $(L_1\sin\theta_0) = Z_{P0}$ and $(L_1\cos\theta_0) = Y_{P0}$, and the expressions simplify to

$$Y_P = Y_{P0} - Z_{P0}\theta \quad (8)$$
$$Z_P = Z_{P0} + Y_{P0}\theta + Z_s \quad (9)$$

The linear system consists of 9 equations with 12 unknowns (coordinates (Y_C, Z_C), (Y_P, Z_P), (Y_Q, Z_Q), (Y_M, Z_M); angles ϕ and θ; and generalized coordinates Z_s and Z_u). The equations can be solved in terms of Z_s, Z_u and ϕ. The Euler-Lagrange will provide two more equations. One more equation is still required, and it will be provided by a link between the camber angle ϕ and the generalized variables Z_s and Z_u.

1) Camber angle: Assume that the camber angle is zero ($\phi = 0$) at the initial position ($Z_u = Z_s = 0$). The simplest approximation is to take $\phi \simeq 0$ for all Z_u and Z_s. More realistic descriptions can be obtained based on system geometry, see e.g. [3] equation (7), or approximations to avoid excessively complex solutions. The 'choice' on ϕ provides a tuning handle for balancing between simplicity and geometric accuracy of the model. Even if $\phi = 0$ seems overly simplistic and 'trivializes' the displacement matrix, it enables to develop some nonlinear characters for the suspension system. A better approximation is obtained with

$$\sin\phi \simeq \phi \simeq \frac{Y_{P0} - Y_P}{L_{03}} \quad (10)$$

based on the system geometry but neglecting the variable component in the strut length.

The 10 equations with 12 unknowns can now be solved

in terms of Z_u and Z_s. In particular, we obtain:

$$\begin{aligned} Y_C &= Y_{C0} + k_C\left(Z_s - Z_u\right) && (11)\\ Z_C &= Z_{C0} + Z_u && (12)\end{aligned}$$

and

$$\begin{aligned} \theta &= k_\theta\left(Z_s - Z_u\right) && (13)\\ \phi &= k_\phi\left(Z_s - Z_u\right) && (14)\end{aligned}$$

For the simple choice $\phi = 0$: $k_C = \frac{Z_{P0}}{Y_{P0}}$, $k_\theta = \frac{-1}{Y_{P0}}$ and $k_\phi = 0$. Choosing (10) the coefficients are $k_C = \gamma Z_{P0}\left(Z_{P0} - z_{C0} + L_{03}\right)$, $k_\theta = \gamma L_{03}$ and $k_\phi = -\gamma Z_{P0}$ with $\gamma^{-1} = Y_{P0}Z_{P0} - Y_{C0}Z_{P0} + Y_{P0}L_{03}$. With these choices, the mappings remain linear.

2) Strut deflection and tyre lateral deflection: In order to construct the Euler-Lagrange equations, some further terms are required. The strut deflection is given by $\delta l = L_3 - L_{03}$, where $L_3 = \sqrt{\left(Y_M - Y_P\right)^2 + \left(Z_M - Z_P\right)^2}$ and $L_{03} = \sqrt{\left(Y_{M0} - Y_{P0}\right)^2 + \left(Z_{M0} - Z_{P0}\right)^2}$. Solving these three equations together with the equations for points M and P in terms of θ: (5),(6), (8) and (9), one obtains

$$\begin{aligned} Y_P &= Y_{P0} - Z_{P0}\theta \\ Z_P &= Z_{P0} + Y_{P0}\theta + Z_s \end{aligned}$$

and

$$L_3 = \sqrt{\left(Y_{P0}^2 + Z_{P0}^2\right)\theta^2 + 2\left(Y_{M0}Z_{P0} - Y_{P0}Z_{M0}\right)\theta + L_{03}^2}$$

A reasonable approximation for small angles is obtained by assuming $\theta^2 \approx 0$:

$$\delta l = \sqrt{L_{03}^2 + k_L\theta} - L_{03} \qquad (15)$$

with $k_L = 2\left(Y_{M0}Z_{P0} - Y_{P0}Z_{M0}\right)$. Equation (15) is non-linear vs. θ.

The tyre lateral deflection due to MacPherson mechanism (under the small angle assumption) is obtained from

$$\delta Y_{tl} = Y_C - Y_{C0} - \phi R$$

(recall that ϕ is positive clockwise), and substituting for Y_C. With (11) and (14) this results in

$$\delta Y_{tl} = \left(k_C - k_\phi R\right)\left(Z_s - Z_u\right) = k_Y\left(Z_s - Z_u\right) \qquad (16)$$

Finally, the deflection between the tyre and the road is:

$$\delta Z_t = Z_u - Z_r \qquad (17)$$

B. Dynamics

The system dynamics are obtained from the Euler-Lagrange equations [4]. Denote kinetic energy by T, potential energy by V and dissipation by D. The Lagrangian relates the kinetic and potential energies, $L = T - V$,

$$\begin{aligned} L &= \frac{1}{2}m_s\left(\dot{Z}_s\right)^2 + \frac{1}{2}m_u\left(\left(\dot{Y}_C\right)^2 + \left(\dot{Z}_u\right)^2\right) \\ &\quad + \frac{1}{2}I_C\left(\dot{\phi}\right)^2 - \frac{1}{2}K_s\left(\delta l\right)^2 \\ &\quad - \frac{1}{2}K_t\left(\delta Z_t\right)^2 - \frac{1}{2}K_{tl}\left(\delta Y_{tl}\right)^2 \end{aligned}$$

where m_s and m_u are the sprung and unsprung masses [kg], I_C the wheel intertia [kg^{2}m], K_s, K_t and K_{tl} are the suspension stiffness and tyre vertical and lateral stifnesses [N/m]. The dissipation D is given by

$$D = \frac{1}{2}B_s(\dot{\delta l})^2 + \frac{1}{2}B_t\left(\delta\dot{Z}_t\right)^2$$

where B_s and B_t are the suspension and tyre damping [Ns/m]. The system dynamics are determined by the Euler-Lagrange equations

$$\begin{aligned} \frac{d}{dt}\left(\frac{\partial L}{\partial \dot{Z}_s}\right) - \frac{\partial L}{\partial Z_s} + \frac{\partial D}{\partial \dot{Z}_s} &= 0 \\ \frac{d}{dt}\left(\frac{\partial L}{\partial \dot{Z}_u}\right) - \frac{\partial L}{\partial Z_u} + \frac{\partial D}{\partial \dot{Z}_u} &= 0 \end{aligned}$$

Calculation of the derivatives for the components in the sums L and D is straightforward. Using (11) and (13)-(17) for ϕ, δl, δY_{tl} and δZ_t we have for L:

$$\begin{aligned} \left(\dot{Y}_C\right)^2 &= k_C^2\left(\dot{Z}_s - \dot{Z}_u\right)^2 \\ \left(\dot{\phi}\right)^2 &= k_\phi^2\left(\dot{Z}_s - \dot{Z}_u\right)^2 \\ \left(\delta l\right)^2 &= \left(L_{03} - \sqrt{L_{03}^2 + k_L k_\theta\left(Z_s - Z_u\right)}\right)^2 \\ \left(\delta Z_t\right)^2 &= \left(Z_r - Z_u\right)^2 \\ \left(\delta Y_{tl}\right)^2 &= k_Y^2\left(Z_s - Z_u\right)^2 \end{aligned}$$

and for D :

$$\begin{aligned} \left(\dot{\delta l}\right)^2 &= \frac{k_L^2 k_\theta^2}{4\left(L_{03}^2 + k_L k_\theta\left(Z_s - Z_u\right)\right)}\left(\dot{Z}_s - \dot{Z}_u\right)^2 \\ \left(\delta\dot{Z}_t\right)^2 &= \left(\dot{Z}_r - \dot{Z}_u\right)^2 \end{aligned}$$

Taking the derivatives leads to the following equations for the MacPherson system:

$$\begin{aligned} m_s\ddot{Z}_s + k_C^2 m_u\left(\ddot{Z}_s - \ddot{Z}_u\right) + I_C k_\phi^2\left(\ddot{Z}_s - \ddot{Z}_u\right) & \\ -K_s F_K\left(Z_s - Z_u\right) & \\ +K_{tl}k_Y^2\left(Z_s - Z_u\right) & \\ +B_s F_B\left(\left(Z_s - Z_u\right), \left(\dot{Z}_s - \dot{Z}_u\right)\right) &= 0 \end{aligned} \qquad (18)$$

$$\begin{aligned} m_u\ddot{Z}_u - m_u k_C^2\left(\ddot{Z}_s - \ddot{Z}_u\right) - I_C k_\phi^2\left(\ddot{Z}_s - \ddot{Z}_u\right) & \\ +K_s F_K\left(Z_s - Z_u\right) & \\ +K_t\left(Z_u - Z_r\right) & \\ -K_{tl}k_Y^2\left(Z_s - Z_u\right) & \\ -B_s F_B\left(\left(Z_s - Z_u\right), \left(\dot{Z}_s - \dot{Z}_u\right)\right) & \\ +B_t\left(\dot{Z}_u - \dot{Z}_r\right) &= 0 \end{aligned} \qquad (19)$$

where

$$\begin{aligned} F_K\left(x\right) &= \frac{k_L k_\theta\left(L_{03} - \sqrt{L_{03}^2 + k_L k_\theta x}\right)}{2\sqrt{L_{03}^2 + k_L k_\theta x}} \\ F_B\left(x, y\right) &= \frac{k_L^2 k_\theta^2 y}{4\left(L_{03}^2 + k_L k_\theta x\right)} \end{aligned}$$

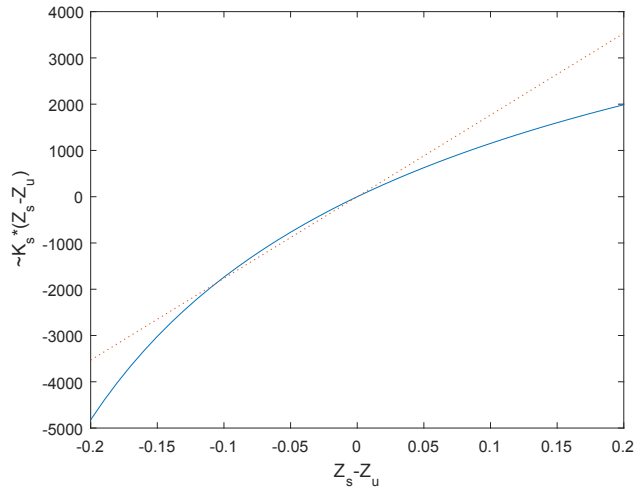

Fig. 3. Nonlinearity of the model: spring.

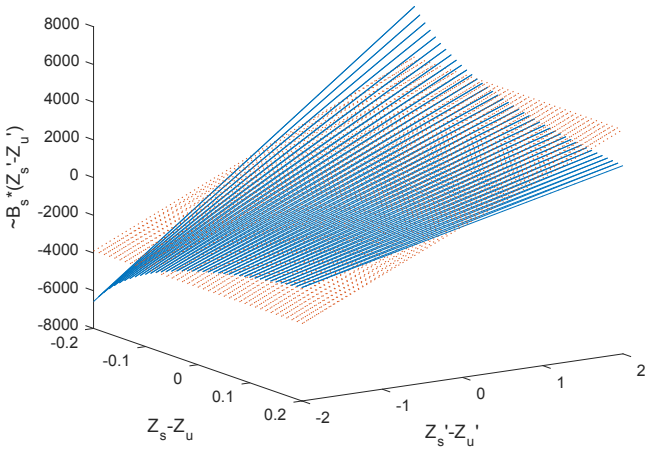

Fig. 4. Model nonlinearity: damping.

The coefficients (k_C, k_θ, k_ϕ and k_L, k_Y) can be obtained from the initial position of the system (see Sec II II-A.1 and II-A.2).

The system is nonlinear due to the terms $F_K\left(Z_s - Z_u\right)$ and $F_B\left(Z_s - Z_u, \dot{Z}_s - \dot{Z}_u\right)$. The model is compact and very easy to simulate given any ode-solver.

III. Simulation analysis

The model, assuming ϕ given by (10), was examined in simulations. Parameters given in Hurel et al. [4] were adopted: $m_s = 453$kg, $m_t = 71$kg, $K_s = 17658$N/m, $B_s = 1950$Ns/m, $K_t = 183887$N/m, $K_{tl} = 50,000$N/m, $B_t = 2500$Ns/m, $R = 0.29$m, and $I_C = 0.021$ kg^{2}m, based on Adams database for MacPherson simulation. The key points are given by $Y_{C0} = 0.3721$m, $Z_{C0} = 0.0275$m, $Y_{Q0} = 0.0000$m, $Z_{Q0} = 0.0000$m, $Y_{M0} = 0.1074$m, $Z_{M0} = 0.5825$m, $Y_{P0} = 0.2490$m, $Z_{P0} = -0.0608$m.

The nonlinearity due to terms F_K and F_B (vs linear) is depicted in Figs. 3-4. At small deflections the gains of the system approach those of the linear system, which approximates the system well when $|Z_s - Z_u| < 0.05$m. The system non-linearities appear as asymmetries for large deflections.

Fig. 5 simulates the system dynamics for a road profile consisting of two pulses (a kerbstrike and a pothole) of amplitude 0.10m. Both the vertical and lateral displacements of the key points {Q, P, C, M} are given by the model. Note that the control arm and camber angles have opposite positive directions and that the strut length (here the distance between points M and P) is given in [dm]. The response of the system appears reasonable. The computation times are very affordable, dictated by solution of the two ode's.

IV. Optimal control design using finite Markov chains

Finite Markov chains and dynamic programming, (a.k.a. Markov Decision Processes, MDP), are powerful tools for design and analysis of dynamic systems [5], [6], [7], and applications [8], [9], [10].

Control with Markov chains is based on a state space description of the system

$$\mathbf{x}(k+1) = f(\mathbf{x}(k), \mathbf{u}(k), \mathbf{w}(k)) \quad (20)$$

$$\mathbf{y}(k) = h(\mathbf{x}(k), \mathbf{v}(k)) \quad (21)$$

where $f : \Re^{n_x} \times \Re^{n_u} \times \Re^{n_w} \longrightarrow \Re^{n_x}$ and $h : \Re^{n_x} \times \Re^{n_v} \longrightarrow \Re^{n_y}$ are nonlinear functions, $\mathbf{w}(k)$ and $\mathbf{v}(k)$ are i.i.d. vectors of random variables with known probability density functions (pdf), and n_x, n_u and n_y are the dimensions of the system state, control and measurement vectors. The goal is that of optimal control, to find a controller such that the anticipated future behavior of the plant will be optimal (*i.e.*, minimize a cost function or maximize profits). Constrats on states and actions can be considered by associating violations with high penalties.

Three important assumptions are underlying the Markov chain approach: i) the system is markovian, ii) the space of the states, actions, and measurements is discretized into a finite set of values, and iii) the cost function has a sequential form, such as $J = \sum c(\mathbf{x}, \mathbf{u})$.

A. Markov transition modelling

In discretization, the state space of $\mathbf{x} \in \mathcal{X}$ is partitioned into s disjoint regions $\mathcal{X}_s$: $\mathcal{X} = \cup_{s=1}^{S} \mathcal{X}_s$ and $\mathcal{X}_s \cap \mathcal{X}_{s'} = \oslash$ $\forall s \neq s'$, $s, s' \in \mathcal{S}$. Many discretization principles can used. In what follows, the cells s are characterized by a set of S centroids and the cell index is determined from a mapping $\mathbf{x} \rightarrow s$:

$$s = \lfloor \arg\min_{s \in \mathcal{S}} \|\mathbf{x} - \mathbf{x}_s^c\|_{\mathbf{W}} \rfloor \quad (22)$$

where $\mathbf{x}_s^c$ are the centroids. $||.||_{\mathbf{W}}$ denotes the Euclidean distance with dimensions of $\mathbf{x}$ weighted by a diagonal $n_x \times n_x$ matrix $\mathbf{W}$, and $\lfloor . \rfloor$ denotes picking the smallest integer in case of multiple optima. Discretization is then determined by the location of the centroids. An efficient

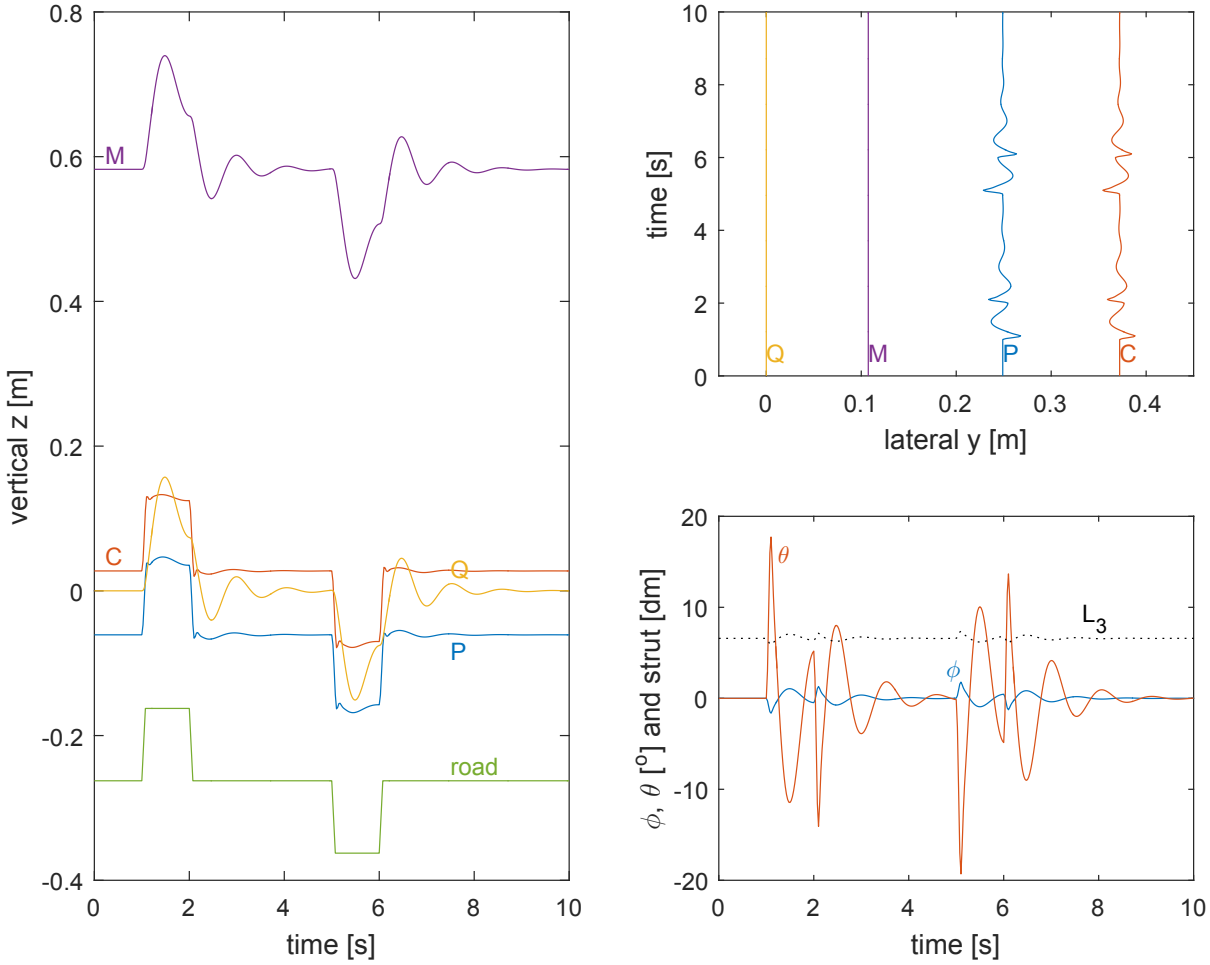

Fig. 5. Free model response in simulations as a function of time. Left: Vertical positions of the key points of the system. Top right: Horizontal coordinates for key points. Bottom right: Angles θ and ϕ and strut length L_3.

approach for discretization was proposed in [11], based on iterative k-means clustering of closed-loop simulation data.

The measurement space can be discretized in a similar way by $\{\mathbf{y}_1, \mathbf{y}_2, ..., \mathbf{y}_M\}$, resulting in (measurement) cells $m \in \mathcal{M} = \{1, 2, ..., M\}$ and $\mathcal{Y} = \cup_{m=1}^{M} \mathcal{Y}_m$. A finite set of A distinct manipulations on how to act on the system is assumed, $\mathbf{u}(k) \in \{\mathbf{u}_1, \mathbf{u}_2, ..., \mathbf{u}_a, ..., \mathbf{u}_A\}$.

The time-evolution of the stochastic state space model can now be described by transitions from $\mathbf{x}(k) \in \mathcal{X}_s$ to $\mathbf{x}(k+1) \in \mathcal{X}_{s'}$ where $s, s' \in \mathcal{S} = \{1, 2, ..., S\}$. This is conveniently described by a transition matrix $\mathbf{P} = [p_{s,s'}]$, where $p_{s,s'}$ is the probability that the system will map to s', if currently in s. This mapping is *a priori* different for each control action $\mathbf{u}_a$, so there will be A such matrices denoted by $\mathbf{P}^a = \left[p^a_{s,s'}\right]$, $a \in \mathcal{A} = \{1, 2, ..., A\}$. The state cell propagation equation

$$\mathbf{q}(k+1) = \mathbf{q}(k)\,\mathbf{P}^{a(k)} \tag{23}$$

is the finite-state version of (20), $\mathbf{q}(k) = [q_s(k)]$ is a row vector of probabilities for the system to occupy cell s at instant k. The finite state version of (21) is given by $\mathbf{o}(k) = \mathbf{q}(k)\,\mathbf{L}(k)$, where $\mathbf{L} = [l_{s,m}]$ and $\mathbf{o}$ is the vector of probabilities for the measurement to occupy cell m.

A major computational effort in building Markov transition models is the construction of the probability transition matrices, $\mathbf{P}^a$. Given a simulation model, the necessary statistics can be built by simply counting the number of observed state-action pairs (s, a) that lead to a particular state s', and normalizing the count by the total number of transitions from the pair.

B. Optimal control design

Suppose that the cost function consists of a sequence of immediate costs

$$J = \sum_{k'=0,1,...,K} \lambda^{k'} c\left(\mathbf{x}(k+k'), \mathbf{u}(k+k')\right) \tag{24}$$

where the indexes in the sum cover a set of time instants in the future horizon. The horizon may be infinitely long, and the costs further in the future may be discounted by λ. These assumptions, together with the finite state and action formulation, allow to use dynamic programming to solve the otherwise easily intractable optimization problem. 'Value iteration' is an iterative algorithm for solving the problem for stationary immediate costs. It will always find the optimal

solution to the minimization of J, and the solution is a look-up table giving the optimal a for each s [6], $a = \pi(s)$.

C. State estimation

In real life applications, noise in system state and measurements is inevitable. The measured variables $\mathbf{y}$ are specified by the measurement equation. The choice of working in discrete spaces enables to feasibly compute the recursive time (prediction) and measurement (update) steps of the Bayesian state estimation. Note that, in general, finding a solution to the Bayesian state estimation problem is intractable in continuous spaces, and only possible under the linear-Gaussian assumptions (Kalman filter). Numerical solutions are possible with, *e.g.*, the particle filters [12], [13], [14], but the on-line computational burden is significant; consequently Extended and Unscented Kalman filtering (EKF, UKF) are more common in practical applications. In a finite state space, the Bayesian state estimation can be written as a cell filter [15]

$$\mathbf{q}(k|k-1) = \mathbf{q}(k-1|k-1)\,\mathbf{P}^{a(k-1)} \quad (25)$$

$$\mathbf{q}(k|k) \sim \mathbf{l}^{\top}{}_{m(k)} \cdot \mathbf{q}(k|k-1) \quad (26)$$

where $\mathbf{l}_{m(k)}$ is the $m(k)$'th column of the likelihood matrix (corresponding to the observation $m(k)$); and $\cdot$ denotes component-wise multiplication. In practice, zero likelihoods may occur due to modelling inaccuracies, in which case the prior predictions can be used to complete posterior probabilities with all states that could result in the observed measurement, and scaling to preserve the probability measure.

The finite state and action stochastic state feedback control problem in its full complexity is considered in partially observable MDP (POMDP) [16], but solutions of the full problem require discretization of the so-called belief space, and have remained unfeasible. In practice, the maximum likelihood approach can be taken, choosing the control action which corresponds to the most likely state $s(k)$, $s(k) = \arg\max_s q_s(k|k)$, $a(k) = \pi(s(k))$. Alternatively, the probability of choosing the correct control action can be maximized:

$$a(k) = \arg\max_a \sum_{s\in\mathcal{S}, a=\pi_s} q_s(k|k) \quad (27)$$

where the summation is over all cell probability masses which result in a control action a.

V. Nonlinear active suspension control

An optimal controller was designed for the active suspension problem using finite Markov chains. Simulations illustrate the behaviour of the closed-loop system.

A. System set-up

The system state vector was given by

$$\mathbf{x} = \left[(Z_s - Z_u), (Z_u - Z_r), \dot{Z}_s, \dot{Z}_u\right]^T$$

the dynamic evolution of which can be obtained from the model (18)-(19). Markov transition models ($\mathbf{P}^a \forall a$, $\mathbf{L}$) were

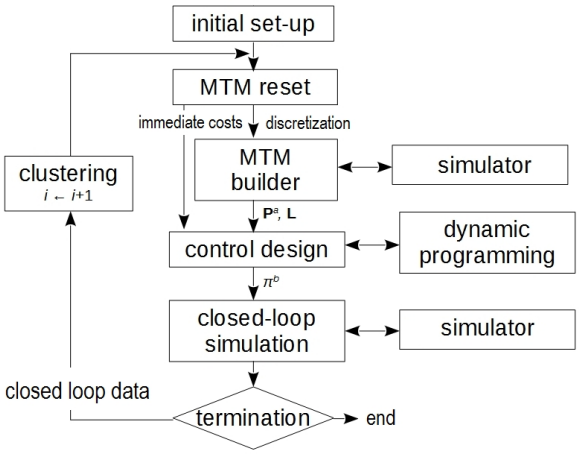

Fig. 6. MDP with iterative discretization.

constructed by exhaustive one-step-ahead simulations of the system using the model, with a sampling time of 25ms. Actions were distributed equally as $\{-4.4, -3.3, ..., 4.4\}$ [kN], $A = 9$. For each state-action pair, E simulations from a random point within the domain of each state cell were constructed, and statistics computed to build the overall state transition matrix. For simplicity, a deterministic control and state estimation problem was considered; a zero road profile was assumed during modelling, $\dot{Z}_r = 0$, the road characteristics were not modelled. The MTM discretization was done iteratively using the iterative k-means approach [11], see Fig. 6 , using weights $\mathbf{W} = [10/9, 5, 1/2, 1/6]$, and solving for the optimal controller using value iteration. The number of clusters ($\approx S$) was gradually increased (+1000 clusters/iteration) as well as the number of evaluations/cell E (+10 evaluations/iteration).

The goal of the active suspension can be expressed in terms of the sprung mass acceleration $\left|\ddot{Z}_s\right|$, suspension deflection $|Z_s - Z_u|$, and the road holding ability $|Z_u - Z_r|$. Assuming an idealized control actuator in the vertical direction, a controller was designed to improve the passive suspension system. The (immediate) cost function was composed as

$$c(\mathbf{x}, \mathbf{u}) = \frac{1}{40}\left|\ddot{Z}_s\right| + \frac{1}{0.3}|Z_s - Z_u| + \frac{1}{0.2}|Z_u - Z_r| \quad (28)$$

where the weighting coefficients adjust the scales of the respective terms in the cost. A discount factor of $\lambda = 0.99$ (i.e., equivalent horizon 100 samples = 2.5 [s]) was used.

In practice, measuring all states is not necessary nor feasible. Therefore, the set of measured variables was taken to be the suspension deflection and sprung mass velocity [17],

$$\mathbf{y} = \begin{bmatrix} 1 & 0 & 0 & 0 \\ 0 & 0 & 1 & 0 \end{bmatrix} \mathbf{x}$$

The measurement space was discretized using a fixed rectangular grid with edges at $[-\infty, -0.233, -0.167, ..., 0.233, \infty]$ for $(Z_s - Z_u)$ and $[-\infty, -1.556, -1.111..., 1.111, \infty]$ for $\dot{Z}_s$ (i.e., $M = 81$). A Bayesian cell filter was designed to

construct the state from the available measurement and past estimate.

Altogether, five controller design iterations (up to $S = 5000$) took a couple of hours of off-line computations, on a modest laptop PC (i5 2.6GHz, Matlab 2015b), where almost all the time was spent in solving the ode's.

B. Simulations

Figure 7 illustrates the active and passive system responses for various bumps and potholes. It can be observed that: the optimal control reduces the cost function to 54% of the passive case, acceleration is reduced 12%, and deflection settling times are reduced to less than half of those of the passive system. Some oscillation remains (see e.g. top right plot), as the small resolution of the finite state/action system did not enable to compensate for such small deviations. Increasing the resolution (M and A) should not pose any problems, but was not tested as the performance was already considered sufficient for illustration purposes. Looking at the motion of the vehicle chassis (top right plot in Fig. 7), the behaviour of the system seems smooth and calm.

VI. Summary and discussion

The paper considered simulation-based non-linear active suspension control design for MacPherson systems. A non-linear dynamic model for the MacPherson suspension system was derived. Simplified kinematics were obtained from system geometry and assuming small angles. The system dynamic equations were derived for two linear approximations of the camber angle using the standard Euler-Lagrange method. The nonlinearities were analyzed, and the dynamic behaviour of the system was illustrated by simulations. The design of controllers and state estimators using finite state Markov models was briefly outlined, and applied for nonlinear active suspension control system.

Albeit nonlinear, the resulting expressions are much simpler than in [3][4], at the expense of loss of details presumably in particular vs the track width and at large angles. The results appeared adequate in terms of modelling performance and computational load, for use in simulation-based design of nonlinear active suspension control systems. Future work should assess the performance of the simplified model vs. other planar and full system models (e.g., via Adams simulations). However, the emphasis of the work was in modeling the vertical dynamics of the sprung mass for active suspension control, and future work should take into account not only more precise kinematics but also the modeling of uncertainties and disturbances associated with the system, as well as the actuator.

The MDP control design example illustrated the power of the finite Markov chains approach in non-linear active suspension control. Significant improvement in closed-loop performance over a passive system was obtained. Major benefits of the MDP-based non-linear control design are in that the computations are off-line, and can be readily extended to consider stochastic components in the system. For simplicity, the simulations assumed an ideal actuator and the system was assumed to be free of state and measurement noise. We expect to report results under stochastic road and measurement noise in the near future.

Active suspension systems provide greatly improved means for improving ride comfort and vehicle handling, but at the same time there are significant drawbacks [1] due to higher energy consumption, cost, complexity and operational requirements due to startup/shutdown, diagnostics and component failures. In the current practice, often only some parameters of the suspension systems are adjusted (semi-active control). In preview control, for example, knowledge of the future road disturbance profile can be used to adjust the stiffness of the shock absorber damping in advance. As pointed out by Tseng and Hrovat [1], main challenges for widespread usage of active suspensions still lies in the area of actuator design and implementation.

Vehicle suspension systems can also be exploited in additional tasks, such as levelling (lowering vehicle at highway speeds), improving safety (cornering), or minimization of road or bridge damages in the case of heavy vehicles. Vehicle-to-vehicle and vehicle-to-infrastucture communications have been proposed recently, e.g., for building up-to-date road maps for preview control [1], and visions on robotic cars and convoys have already been demonstrated in practice. Indeed, there are a number of interesting links between the 'basic low-level' problem of suspension control and the tasks at higher level optimization of transportation systems.

Acknowledgements

This work was conducted during the visit of E. Ikonen to Department of Systems and Automation Engineering at the University of Malaga, Spain. Financial support from the Foundations' Professor Pool (Suomen Kulttuurirahasto, Kalle ja Dagmar Välimaan rahasto) is gratefully acknowledged.

References

[1] H. E. Tsang and D. Hrovat, "State of the art survey: active and semi-active suspension control," *Vehicle System Dynamics*, vol. 53, no. 7, pp. 1034–1062, 2015.

[2] J. Cao, H. Liu, P. Li, and D. Brown, "State of the art in vehicle active suspension adaptive control systems based on intelligent methodologies," *IEEE Transactions on Intelligent Transportation Systems*, vol. 9, no. 3, pp. 392 – 405, 2008.

[3] M. S. Fallah, R. Bhat, and W. F. Xie, "New model and simulation of macpherson suspension system for ride control applications," *Vehicle System Dynamics*, vol. 47, no. 2, pp. 195–220, 2009.

[4] J. Hurel, A. Mandow, and A. Garcia-Cerezo, "Kinematic and dynamic analysis of the mcpherson suspension with a planar quarter-car model," *Vehicle System Dynamics*, vol. 51, no. 9, pp. 1422–1437, 2013.

[5] J. Kemeny and J. Snell, *Finite Markov chains*. New York: van Nostrand, 1960.

[6] M. L. Puterman, *Markov Decision Process - Discrete Stochastic Dynamic Programming*. Wiley-Interscience, 1994.

[7] C. S. Hsu, *Cell-to-cell mapping - a method of global analysis for nonlinear systems*. Springer Verlag, 1987.

[8] W. J. Powell, *Approximate dynamic programming - Solving the curses of dimensionality*. Wiley-Interscience, 2010.

[9] D. J. White, "A review of applications of Markov decision processes," *Journal of the operational research society*, vol. 44, no. 11, pp. 1073–1096, 1989.

[10] E. Ikonen and K. Najim, "Multiple model-based control using finite control Markov chains," *Cognitive Computation*, vol. 1, pp. 234–243, 2009.

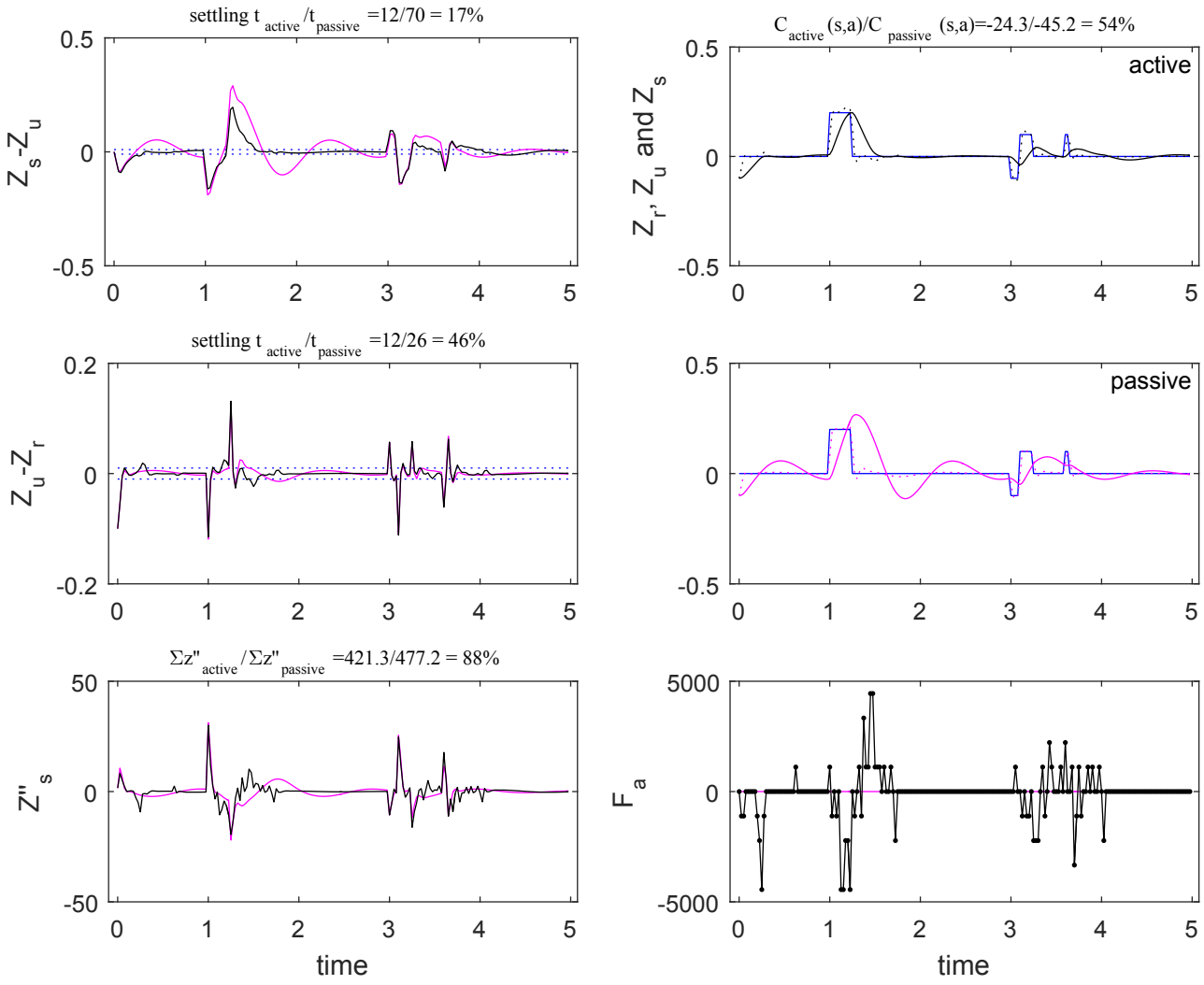

Fig. 7. Response under active/passive control. Left plots from top to bottom: suspension deflection, tyre deflection and sprung mass acceleration. Right plots top and middle: Sprung and unsprung mass deplacements; bottom: and active control force. Black lines: active system, magenta lines: passive system.

[11] E. Ikonen, I. Selek, and K. Najim, "Process control using finite Markov chains with iterative clustering," *Computers & Chemical Engineering*, vol. 93, pp. 293–308, 2016.

[12] N. J. Gordon, D. J. Salmond, and A. F. M. Smith, "Novel approach to nonlinear/non-Gaussian Bayesian state estimation," *IEE Proceedings*, vol. 140, no. 2, pp. 107–113, 1993.

[13] M. Arulampalam, S. Maskell, N. Gordon, and T. Clapp, "A tutorial on particle filter for online/non-Gaussian Bayesian tracking," *IEEE Transactions on Signal Processing*, vol. 50, no. 2, pp. 174–188, 2002.

[14] E. Ikonen, J. Kovacs, and J. Ritvanen, "Circulating fluidized bed hot-loop analysis, tuning and state estimation using particle filtering," *International Journal of Innovative Computing, Information and Control*, vol. 9, no. 8, pp. 3357–3376, 2013.

[15] S. Ungarala, Z. Chen, and K. Li, "Bayesian state estimation of non-linear systes using approximate aggregate Markov chains," *Industrial & Engineering Chemistry Research*, vol. 45, pp. 4208–4221, 2006.

[16] L. P. Kaelbling, M. L. Littman, and A. R. Cassandra, "Planning and acting in partially observable stochastic domains," *Artificial Intelligence*, vol. 101, pp. 99–134, 1998.

[17] S.-Y. Han, Y.-H. Chen, K. Ma, D. Wang, A. Abraham, and Z.-G. Liu, "Feedforward and feedback optimal vibration rejection for active suspension discrete-time systems under in-vehicle networls," in *2014 6th World Congress on Nature and Biologically Inspired Computing (NaBIC)*, 2014, pp. 139–144.